First- and Second-Order Topological Superconductivity and Temperature-Driven Topological Phase Transitions in the Extended Hubbard Model with Spin-Orbit Coupling

Majid Kheirkhah,[1,*] Zhongbo Yan,[2] Yuki Nagai,[3,4] and Frank Marsiglio[1]
[1]*Department of Physics, University of Alberta, Edmonton, Alberta T6G 2E1, Canada*
[2]*School of Physics, Sun Yat-Sen University, Guangzhou 510275, China*
[3]*CCSE, Japan Atomic Energy Agency, 178-4-4, Wakashiba, Kashiwa, Chiba 277-0871, Japan*
[4]*Mathematical Science Team, RIKEN Center for Advanced Intelligence Project (AIP), 1-4-1 Nihonbashi, Chuo-ku, Tokyo 103-0027, Japan*

(Received 23 January 2020; accepted 2 June 2020; published 30 June 2020)

The combination of spin-orbit coupling with interactions results in many exotic phases of matter. In this Letter, we investigate the superconducting pairing instability of the two-dimensional extended Hubbard model with both Rashba and Dresselhaus spin-orbit coupling within the mean-field level at both zero and finite temperature. We find that both first- and second-order time-reversal symmetry breaking topological gapped phases can be achieved under appropriate parameters and temperature regimes due to the presence of a favored even-parity $s + id$-wave pairing even in the absence of an external magnetic field or intrinsic magnetism. This results in two branches of chiral Majorana edge states on each edge or a single zero-energy Majorana corner state at each corner of the sample. Interestingly, we also find that not only does tuning the doping level lead to a direct topological phase transition between these two distinct topological gapped phases, but also using the temperature as a highly controllable and reversible tuning knob leads to different direct temperature-driven topological phase transitions between gapped and gapless topological superconducting phases. Our findings suggest new possibilities in interacting spin-orbit coupled systems by unifying both first- and higher-order topological superconductors in a simple but realistic microscopic model.

DOI: 10.1103/PhysRevLett.125.017001

Introduction.—Spin-orbit coupling (SOC) is ubiquitous in condensed matter systems and responsible for many remarkable phenomena [1–16]. In recent years, a surge of research interest in SOC was stimulated by the discovery that SOC plays a critical role in realizing various topological phases, ranging from noninteracting or weakly correlated topological insulators (TIs) and topological superconductors (TSCs) to strongly correlated topological phases [17–20]. Among them, TSCs are noticeable as they harbor Majorana modes, which are believed to be a possibility for the building blocks of topological quantum computation [21–25]. While odd-parity superconductors generally provide a natural realization of TSCs [26–31], their scarcity in nature turns out to be a serious obstacle from an experimental point of view. Fortunately, SOC enables the realization of effective odd-parity superconductivity (SC) on the basis of abundant even-parity SC, providing a more readily accessible route for the realization of TSCs [32–39]. Over the past decade, remarkable progress along this route has been witnessed [40–48].

Very recently, a new class of topological phases, named higher-order TIs and TSCs, have emerged and attracted a great deal of attention because of the enrichment of boundary physics and the occurrence of new possibilities for topological phase transitions [49–64]. The word "order" in this context gives the codimension of the gapless boundary modes, namely, an nth order TI or TSC has gapless boundary modes with codimension n. As the gapless boundary modes of all conventional TIs and TSCs have $n = 1$, they thus belong to the first-order topological phases in this language.

Because higher-order TSCs provide new platforms of Majorana modes, their potential application in topological quantum computation has triggered quite a few theoretical proposals on their experimental realizations [65–89]. However, the superconducting pairings in previous works were mostly introduced phenomenologically, and realistic microscopic models for higher-order TSCs are still generally lacking. Over the past decade, the Hubbard model with SOC and on site interaction, as one of the simplest microscopic models for first-order TSCs, has been extensively studied in both condensed matter and in the cold atom communities [90–96]. In this Letter, we extend the Hubbard model in two dimensions to include both on site (repulsive) and intersite (attractive) interactions and investigate its even-parity superconducting pairing instability at the mean-field level [97].

Our study reveals that depending on the temperature and the parameters of the model, the leading pairing channel can be d-, s-, or $s + id$-wave [98,99]. Remarkably, we find when the $s + id$-wave is favored, a first-order TSC with two branches of chiral edge states and a second-order TSC with four Majorana corner modes, as well as a direct topological phase transition between them, can be realized by tuning the Fermi surface (FS) structure, even in the absence of a magnetic field or magnetism. Furthermore, we show that the temperature itself is a highly controllable and reversible tuning knob to drive topological phase transitions in this system.

Theoretical formalism.—The two-dimensional extended Hubbard model, which provides a simple description for short-ranged interacting systems [97], reads as

$$\begin{aligned} H = & -t\sum_{\langle i,j\rangle,\alpha} c^\dagger_{i,\alpha}c_{j,\alpha} + \text{H.c.} - \mu\sum_{i,\alpha} c^\dagger_{i,\alpha}c_{i,\alpha} \\ & + i\lambda_R\sum_{i,\alpha,\beta}(c^\dagger_{i,\alpha}s_y^{\alpha\beta}c_{i+\hat{x},\beta} - c^\dagger_{i,\alpha}s_x^{\alpha\beta}c_{i+\hat{y},\beta}) + \text{H.c.} \\ & + i\lambda_D\sum_{i,\alpha,\beta}(c^\dagger_{i,\alpha}s_y^{\alpha\beta}c_{i+\hat{y},\beta} - c^\dagger_{i,\alpha}s_x^{\alpha\beta}c_{i+\hat{x},\beta}) + \text{H.c.} \\ & + U\sum_i \hat{n}_{i,\uparrow}\hat{n}_{i,\downarrow} + \frac{V}{2}\sum_{i,j,\alpha}\hat{n}_{i,\alpha}\hat{n}_{j,\bar{\alpha}}, \end{aligned} \tag{1}$$

where $\langle i,j\rangle$ denotes summation over nearest-neighbor sites, $c^\dagger_{i,\alpha}(c_{i,\alpha})$ is the creation (annihilation) operator at site i with spin $\alpha = (\uparrow,\downarrow)$, $\hat{n}_{i,\alpha} = c^\dagger_{i,\alpha}c_{i,\alpha}$, t is the nearest-neighbor hopping amplitude, μ is the chemical potential, λ_R (λ_D) is the Rashba (Dresselhaus) SOC amplitude, U is the on site repulsive ($U > 0$) interaction strength, and V is the nearest-neighbor attractive ($V < 0$) interaction strength. The unit vector along the x (y) direction is represented by $\hat{x}$ ($\hat{y}$), and $s_{x,y}$ are Pauli matrices in spin space. The abbreviation H.c. stands for Hermitian conjugation, and the symbol i in the beginning of both second and third lines (and elsewhere) is taken to denote the pure imaginary number and should not be confused with the site index which generally occurs as subscripts.

Although in the presence of SOC, odd- and even-parity pairings can generally coexist, we restrict ourselves to even-parity pairing for the sake of clarity and simplicity. Accordingly, the Bogoliubov–de Gennes (BdG) Hamiltonian at the mean-field level in momentum space (see Supplemental Material [100]) can be rewritten as $H = \frac{1}{2}\sum_{\boldsymbol{k}}\Psi^\dagger_{\boldsymbol{k}}\mathcal{H}(\boldsymbol{k})\Psi_{\boldsymbol{k}}$, with $\Psi^T_{\boldsymbol{k}} = (c_{\boldsymbol{k}\uparrow}, c_{\boldsymbol{k}\downarrow}, c^\dagger_{-\boldsymbol{k}\downarrow}, -c^\dagger_{-\boldsymbol{k}\uparrow})$ and

$$\mathcal{H}(\boldsymbol{k}) = \tau_z\{\xi(\boldsymbol{k})s_0 + l_x(\boldsymbol{k})s_x + l_y(\boldsymbol{k})s_y\} + \Delta(\boldsymbol{k})\tau_x s_0, \tag{2}$$

where $\tau_{x,y,z}$ are Pauli matrices in particle-hole space, and $\xi_{\boldsymbol{k}} = -2t(\cos k_x + \cos k_y) - \mu$ is the kinetic energy measured from the Fermi energy; $\boldsymbol{l}(\boldsymbol{k}) = (l_x(\boldsymbol{k}), l_y(\boldsymbol{k}))$ is the SOC vector, with $\boldsymbol{l}(\boldsymbol{k}) = \boldsymbol{l}_R(\boldsymbol{k}) + \boldsymbol{l}_D(\boldsymbol{k})$, where $\boldsymbol{l}_R(\boldsymbol{k}) = 2\lambda_R(\sin k_y, -\sin k_x)$ and $\boldsymbol{l}_D(\boldsymbol{k}) = 2\lambda_D(\sin k_x, -\sin k_y)$ represents the Rashba and Dresselhaus SOC, respectively. The superconducting order parameter is given by

$$\Delta(\boldsymbol{k}) = \Delta_0^c + \Delta_s^c\eta_s(\boldsymbol{k}) + \Delta_d^c\eta_d(\boldsymbol{k}), \tag{3}$$

where Δ_0^c, Δ_s^c, and Δ_d^c are momentum-independent complex numbers that represent on site s-, extended s-, and d-wave SC, respectively. The three pairing amplitudes satisfy the following self-consistent superconducting gap equations:

$$\Delta_0^c = -\frac{U}{4N}\sum_{\boldsymbol{k},\sigma}\Delta(\boldsymbol{k})\mathcal{F}_\sigma(\boldsymbol{k}), \tag{4}$$

$$\Delta_s^c = -\frac{V}{N}\sum_{\boldsymbol{k},\sigma}\Delta(\boldsymbol{k})\eta_s(\boldsymbol{k})\mathcal{F}_\sigma(\boldsymbol{k}), \tag{5}$$

$$\Delta_d^c = -\frac{V}{N}\sum_{\boldsymbol{k},\sigma}\Delta(\boldsymbol{k})\eta_d(\boldsymbol{k})\mathcal{F}_\sigma(\boldsymbol{k}), \tag{6}$$

where N denotes the number of sites, $\sigma = \pm 1$, $\eta_s(\boldsymbol{k}) = (\cos k_x + \cos k_y)/2$, $\eta_d(\boldsymbol{k}) = (\cos k_x - \cos k_y)/2$, and

$$\mathcal{F}_\sigma(\boldsymbol{k}) = \frac{1}{E^\sigma_{\boldsymbol{k}}}\tanh\left(\frac{\beta E^\sigma_{\boldsymbol{k}}}{2}\right). \tag{7}$$

Here β is the inverse of temperature and

$$E^\sigma_{\boldsymbol{k}} = \sqrt{\varepsilon^2_\sigma(\boldsymbol{k}) + |\Delta(\boldsymbol{k})|^2} \tag{8}$$

are the two excitation spectra of the BdG Hamiltonian, where $\varepsilon_\sigma(\boldsymbol{k}) = \xi(\boldsymbol{k}) + \sigma l(\boldsymbol{k})$ refers to the normal-state spectra with $l(\boldsymbol{k})$ the magnitude of the $\boldsymbol{l}(\boldsymbol{k})$ vector.

To capture the phases of the three pairings, we define $\Delta^c_\alpha = \Delta_\alpha e^{i\phi_\alpha}$ for $\alpha \in \{0, s, d\}$, with Δ_α and ϕ_α being real numbers. Accordingly, the three complex self-consistent equations given by Eqs. (4)–(6) can be separated into six real equations. By solving the self-consistent equations numerically, we find that, when both s- and d-wave superconducting order parameters are nonvanishing, their phases favor $\phi_s = \phi_0$ and $\phi_d = \phi_0 \pm \pi/2$ ("$\pm$" are degenerate in energy). Therefore, the superconducting order parameter can be written explicitly as

$$\Delta(\boldsymbol{k}) = \Delta_0 + \Delta_s\eta_s(\boldsymbol{k}) + i\Delta_d\eta_d(\boldsymbol{k}), \tag{9}$$

and, accordingly, the six real self-consistent superconducting gap equations are reduced to

$$\Delta_0 = -\frac{U}{4N}\sum_{\boldsymbol{k},\sigma}\{\Delta_0 + \Delta_s\eta_s(\boldsymbol{k})\}\mathcal{F}_\sigma(\boldsymbol{k}), \tag{10}$$

$$\Delta_s = -\frac{V}{N}\sum_{\boldsymbol{k},\sigma}\eta_s(\boldsymbol{k})\{\Delta_0 + \Delta_s\eta_s(\boldsymbol{k})\}\mathcal{F}_\sigma(\boldsymbol{k}), \tag{11}$$

$$1 = -\frac{V}{N}\sum_{\boldsymbol{k},\sigma}\eta_d^2(\boldsymbol{k})\mathcal{F}_\sigma(\boldsymbol{k}). \tag{12}$$

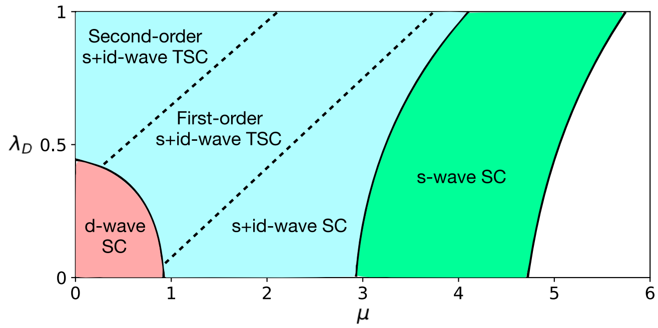

FIG. 1. Zero-temperature phase diagram for $\{t, \lambda_R, U, V\} = \{1, 0.3, 2, -5\}$. The phase diagram contains d-wave SC (red color region), $s + id$-wave SC (blue color region), and s-wave SC (green color region). The time-reversal symmetry breaking $s + id$-wave SC phase consists of three topologically distinct phases, including first- and second-order TSC and topologically trivial SC.

It should be noted that, when s- and d-wave pairing coexist, the last term of the BdG Hamiltonian (2) should be rewritten as $\{[\Delta_0 + \Delta_s\eta_s(\boldsymbol{k})]\tau_x - \Delta_d\eta_d(\boldsymbol{k})\tau_y\}s_0$. Throughout this Letter, we set the hopping amplitude $t = 1$ as the energy unit and $\{\lambda_R, U, V\} = \{0.3, 2, -5\}$, unless we clearly mention otherwise. However, they are not unique, and different sets of parameters will yield a qualitatively similar phase diagram.

Results.—We first perform the self-consistent calculations at zero temperature. For definiteness, we consider that only λ_D and μ are tunable parameters. We restrict ourselves to the positive parameter regime and present the corresponding phase diagram in Fig. 1. The result reveals the existence of three distinct types of pairing, including time-reversal symmetry (TRS) preserving s- and d-wave, as well as the TRS breaking $s + id$-wave. The s- and $s + id$-wave pairing regimes are gapped except at some critical lines and points, respectively [101], while the d-wave pairing regime corresponds to a nodal superconducting phase, since it cannot open a bulk gap. Moreover, the TRS preserving gapped s-wave pairing belongs to the symmetry class DIII characterized by a $\mathbb{Z}_2$ invariant ν [102,103] and the TRS preserving gapless d-wave pairing is considered as a topologically nontrivial phase, though gapless, because it harbors topologically protected gapless Majorana modes on the boundary.

Let us now focus on the interesting regime with $s + id$-wave pairing, which consists of three TRS breaking topologically distinct phases, including first- and second-order TSC and topologically trivial SC, as shown in the blue color region of Fig. 1. Since the TRS is broken in this regime, the system belongs to the symmetry class D characterized by the Chern number [104]. To reveal the underlying topological property in a simple and transparent way, here we perform a basis transformation that maps the combination of SOC and even-parity $s + id$-wave pairing to an effective odd-parity pairing [37]. After the transformation (see Supplemental Material [100]), the four-band BdG Hamiltonian can be decoupled into two independent parts, i.e., $\mathcal{H}(\boldsymbol{k}) = \mathcal{H}_+(\boldsymbol{k}) \oplus \mathcal{H}_-(\boldsymbol{k})$, with

$$\mathcal{H}_\pm(\boldsymbol{k}) = \begin{pmatrix} |\xi_k| \pm l(\boldsymbol{k}) & \Delta_\pm(\boldsymbol{k}) \\ \Delta_\pm^*(\boldsymbol{k}) & -|\xi_k| \mp l(\boldsymbol{k}) \end{pmatrix}, \qquad (13)$$

where $\Delta_\pm(\boldsymbol{k}) = [\Delta_0 + \Delta_s\eta_s(\boldsymbol{k}) \mp i\Delta_d\eta_d(\boldsymbol{k})](l_x \mp il_y)/l(\boldsymbol{k})$. It is apparent that $\Delta_\pm(-\boldsymbol{k}) = -\Delta_\pm(\boldsymbol{k})$, confirming the odd-parity nature. As is known, the band topology of an odd-parity superconductor is determined by the relative configuration of the FSs and the pairing nodes, and there exists a simple relation between the Chern number (C) and the number of FSs (N_F) enclosing one time-reversal invariant point, which is $(-1)^C = (-1)^{N_F}$ [26,105]. The number of FSs of $\mathcal{H}(\boldsymbol{k})$ must be even since the normal state has TRS, which implies that C must be an even integer. In addition, the gapped energy spectra of $\mathcal{H}_+(\boldsymbol{k})$ implies the absence of a FS, which is defined as the constant-energy contour satisfying $|\xi_k| + l(\boldsymbol{k}) = 0$, while $\mathcal{H}_-(\boldsymbol{k})$ has either zero or two FSs, depending on the chemical potential μ. As the absence of FSs always implies a trivial superconductor, only the situation that $\mathcal{H}_-(\boldsymbol{k})$ has two FSs is of interest. When C is a nonzero even integer, the system corresponds to a first-order TSC with C branches of Majorana chiral edge states. However, when $C = 0$, the system is either a topologically trivial superconductor or a second-order TSC, depending on whether the two FSs of $\mathcal{H}_-(\boldsymbol{k})$ can be continuously deformed to annihilate with each other without crossing any removable Dirac pairing nodes (not at time-reversal invariant points) or not.

Interestingly, we notice that $\mathcal{H}_-(\boldsymbol{k})$ takes a form similar to the toy model realizing second-order TSC proposed in Ref. [76]. Here, there are four removable Dirac pairing nodes whose net sum of winding number [defined as $\omega = (1/2\pi i)\oint \Delta_-^{-1}\partial_k\Delta_- dk$, with the closed integration contour enclosing only the interested pairing node] is zero lying between the two FSs, the system realizes a second-order TSC. Another way to understand this picture is via the edge theory. To be specific, when the four removable Dirac pairing nodes of $\mathcal{H}_-(\boldsymbol{k})$ lie between the two FSs, it means that, if we neglect the d-wave pairing, the line nodes of s-wave pairing (satisfying $\Delta_0 + \Delta_s\eta_s = 0$) can be chosen to lie between the two FSs. Since without the d-wave pairing, the full Hamiltonian restores the TRS, then according to the formula $\nu = \prod_i[\mathrm{sgn}(\Delta_i)]^{m_i}$ [102] we have $\nu = -1$, indicating the realization of a first-order time-reversal invariant TSC that hosts a pair of helical Majorana edge states. Bringing back the d-wave pairing, the helical edge states are gapped out due to the breaking of TRS. However, as the d-wave pairing itself has line nodes along the directions $k_x = \pm k_y$, four Majorana zero modes will be left at the four corners when we use open-boundary conditions in both x and y directions [67,69].

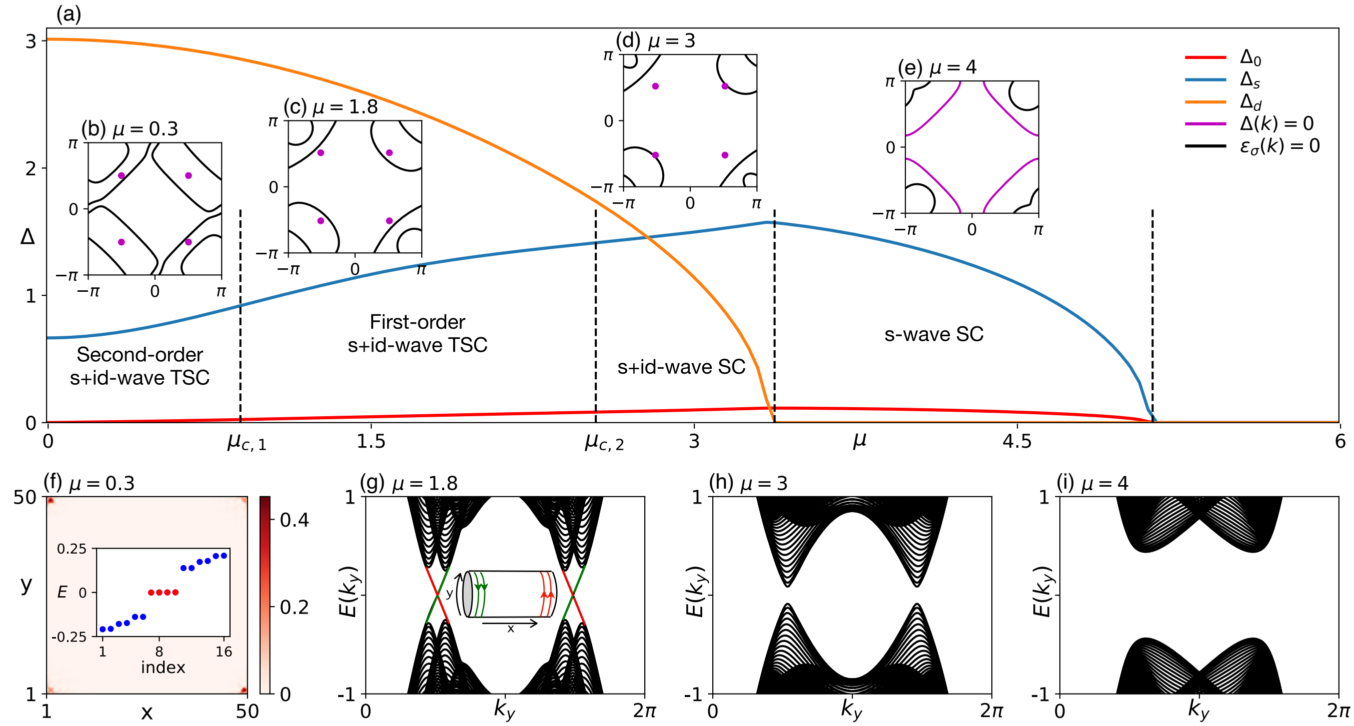

FIG. 2. Common parameters: $\{t, \lambda_R, \lambda_D, U, V\} = \{1, 0.3, 0.6, 2, -5\}$. (a) The dependence of $\Delta_{0,s,d}$ on μ at zero temperature. The dashed lines perpendicular to the μ axis correspond to phase boundaries. The four insets (b)–(e) show four representative configurations of FSs (black) and pairing nodes (purple points or lines) in the four distinct phases. (b) $\mu = 0.3$, (c) $\mu = 1.8$, (d) $\mu = 3$, and (e) $\mu = 4$ [for this value, one of the FS becomes a point at (π, π)]. (f) The probability density profiles of four Majorana corner states (red points of the inset) and the eigenvalues of the BdG Hamiltonian around zero energy in real space for a 50×50 square lattice with open-boundary conditions in both x and y directions. (g)–(i) Energy spectrum for cylindrical geometry with open-boundary condition only along the x direction. The inset of (g) shows the distribution of chiral Majorana edge states in real space.

Based on the above analysis, we find that, within the $s + id$-wave pairing regime, the change of topology only takes place when the FSs cross the removable Dirac pairing nodes at which both $\Delta_0 + \Delta_s \eta_s = 0$ and $\Delta_d \eta_d = 0$ are simultaneously fulfilled. As for the parameters considered, we find $\Delta_0 \ll \Delta_s, \Delta_d$; these nodes are almost fixed at the four points $\mathbf{Q}_{\pm,\pm} = (\pm\pi/2, \pm\pi/2)$. Therefore, the condition for topological phase transitions can be very accurately described by the normal-state condition $|\xi_{\mathbf{Q}_{\pm,\pm}}| - l(\mathbf{Q}_{\pm,\pm}) = 0$. It is straightforward to find that the solutions give two straight lines satisfying $|\mu| - 2\sqrt{2}|\lambda_R \pm \lambda_D| = 0$ (see Supplemental Material [100]), which correspond to the two dashed lines in the blue color region of Fig. 1.

To support the above analysis, we further diagonalize the mean-field BdG Hamiltonian in real space (see Supplemental Material [100]). To be specific, we fix $\lambda_D = 0.6$ and study the evolution of boundary modes with μ. The results are presented in Fig. 2. In accordance with the phase diagram in Fig. 1, we know that $\mu_{c,1} \simeq 3\sqrt{2}/5 \simeq 0.85$ and $\mu_{c,2} \simeq 9\sqrt{2}/5 \simeq 2.55$ are two critical points in the regime with $s + id$-wave pairing [100]. Within each phase, we show one representative configuration of FSs and pairing nodes [Figs. 2(b)–2(e)]. Figure 2(b) shows that, within the regime $0 < \mu < \mu_{c,1}$, the four pairing nodes at $(\pm\pi/2, \pm\pi/2)$ are located between the two concentric FSs enclosing (π, π), indicating the realization of a second-order TSC [76]. To demonstrate this phase, we consider a square sample with open-boundary conditions in both x and y directions. A diagonalization of the real-space Hamiltonian does confirm the existence of four Majorana corner modes [see Fig. 2(f)] and, therefore, the realization of a second-order TSC. Within the regime $\mu_{c,1} < \mu < \mu_{c,2}$, only two of the four pairing nodes at $(\pm\pi/2, \pm\pi/2)$ remain to be located between the two FSs, as shown in Fig. 2(c). As one pairing node takes the same winding number as its inversion partner, the transition from the configuration in Fig. 2(b) to that in Fig. 2(c) suggests a change of Chern number by two. In other words, a first-order TSC with $C = 2$ is realized in the regime $\mu_{c,1} < \mu < \mu_{c,2}$. To demonstrate this phase, we consider a cylinder geometry with open-boundary conditions only along the x direction. The numerical result confirms the existence of two chiral Majorana modes on each edge [see Fig. 2(g)] and, therefore, the realization of a first-order TSC with $C = 2$. Remarkably, the above results suggest that a topological phase transition between second- and first-order TSCs takes place at $\mu_{c,1}$ [106]. Numerical calculations reveal

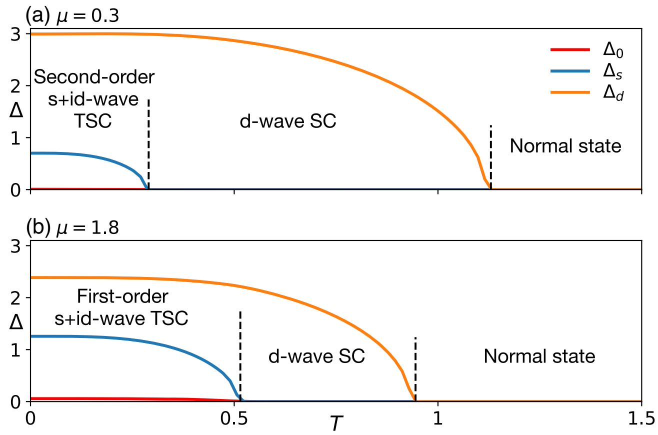

FIG. 3. Temperature-driven topological phase transitions. $\{t,\lambda_R,\lambda_D,U,V\}=\{1,0.3,0.6,2,-5\}$, and (a) $\mu=0.3$, (b) $\mu=1.8$. Tuning the temperature can change both the favored pairing and the underlying topology.

the absence of gapless boundary modes [Figs. 2(h) and 2(i)] in the regime $\mu > \mu_{c,2}$, indicating that the Hamiltonian is trivial in topology in this regime.

So far, we have restricted the results to the zero-temperature limit. By performing self-consistent calculations at finite temperature, we find that, for a given configuration of FSs, different pairing types exhibit different temperature dependence. As a result, the favored pairing can undergo a dramatic change at some critical temperature. To be specific, Fig. 3 shows two examples whose ground states at zero temperature are second- and first-order $s + id$-wave TSCs. From this figure, it is readily seen that the increase of temperature leads to a change of the favored pairing from gapped $s + id$-wave TSC to d-wave gapless SC at a parameter-dependent critical temperature. Since the d-wave pairing leads to the realization of nodal or Dirac SC, it indicates that the temperature itself provides a way to tune the underlying topological properties.

Conclusions.—In this Letter, we showed that both first- and second-order TRS breaking topological superconductivity as well as the topological phase transition between them can emerge in the extended Hubbard model with both Rashba and Dresselhaus SOC, even in the absence of an external magnetic field or magnetic order. Moreover, we demonstrated that, with appropriate FS structure, tuning only the temperature can result in interesting topological phase transitions in this system. Our findings are relevant to many systems where both SOCs and interactions are tunable, including InSb [37] or InGaAs [107] quantum wells in proximity to a high-temperature iron-based superconductor, which has an order parameter with $s + id$-wave superconducting pairing symmetry [108–110], oxide interfaces like $LaAlO_3/SrTiO_3$ [111,112], and cold atom systems [113].

This work was supported in part by the Natural Sciences and Engineering Research Council of Canada (NSERC). Z. Y. is supported by Startup Grant of Sun Yat-sen University (Grant No. 74130-18841219) and NSFC-11904417. Y. N. was partially supported by JSPS KAKENHI Grants No. 18K11345 and No. 18K03552, the "Topological Materials Science" (Grant No. JP18H04228) KAKENHI on Innovative Areas from JSPS of Japan.

*Corresponding author.
kheirkhah@ualberta.ca

[1] E. I. Rashba, Symmetry of energy bands in crystals of wurtzite-type: I. Symmetry of bands disregarding spin-orbit interaction, Sov. Phys. Solid State **1**, 368 (1959).
[2] E. I. Rashba and V. I. Sheka, Symmetry of energy bands in crystals of wurtzite type: II. Symmetry of bands with spin-orbit interaction included, Fiz. Tverd. Tela: Collected Papers **2**, 62 (1959), https://dash.harvard.edu/handle/1/29426010.
[3] R. J. Elliott, Spin-orbit coupling in band theory—character tables for some "double" space groups, Phys. Rev. **96**, 280 (1954).
[4] G. Dresselhaus, A. F. Kip, and C. Kittel, Spin-orbit interaction and the effective masses of holes in Germanium, Phys. Rev. **95**, 568 (1954).
[5] G. Dresselhaus, Spin-orbit coupling effects in Zinc Blende structures, Phys. Rev. **100**, 580 (1955).
[6] G. Dresselhaus, A. F. Kip, and C. Kittel, Cyclotron resonance of electrons and holes in Silicon and Germanium crystals, Phys. Rev. **98**, 368 (1955).
[7] S. D. Ganichev and L. E. Golub, Interplay of Rashba/Dresselhaus spin splittings probed by photogalvanic spectroscopy—A review, Phys. Status Solidi (b) **251**, 1801 (2014).
[8] A. Manchon, H. C. Koo, J. Nitta, S. M. Frolov, and R. A. Duine, New perspectives for Rashba spin-orbit coupling, Nat. Mater. **14**, 871 (2015).
[9] G. Bihlmayer, O. Rader, and R. Winkler, Focus on the Rashba effect, New J. Phys. **17**, 050202 (2015).
[10] L. P. Gor'kov and E. I. Rashba, Superconducting 2D System with Lifted Spin Degeneracy: Mixed Singlet-Triplet State, Phys. Rev. Lett. **87**, 037004 (2001).
[11] P. A. Frigeri, D. F. Agterberg, A. Koga, and M. Sigrist, Superconductivity without Inversion Symmetry: MnSi Versus $CePt_3Si$, Phys. Rev. Lett. **92**, 097001 (2004).
[12] V. M. Edelstein, Magnetoelectric Effect in Polar Superconductors, Phys. Rev. Lett. **75**, 2004 (1995).
[13] M. H. Fischer, M. Sigrist, and D. F. Agterberg, Superconductivity without Inversion and Time-Reversal Symmetries, Phys. Rev. Lett. **121**, 157003 (2018).
[14] Y. Nagai, S. Hoshino, and Y. Ota, Critical temperature enhancement of topological superconductors: A dynamical mean-field study, Phys. Rev. B **93**, 220505(R) (2016).
[15] S. L. Goertzen, K. Tanaka, and Y. Nagai, Self-consistent study of Abelian and non-Abelian order in a two-dimensional topological superconductor, Phys. Rev. B **95**, 064509 (2017).
[16] V. Galitski and I. B. Spielman, Spin-orbit coupling in quantum gases, Nature (London) **494**, 49 (2013).

[17] J. E. Moore, The birth of topological insulators, Nature (London) **464**, 194 (2010).
[18] D. Pesin and L. Balents, Mott physics and band topology in materials with strong spin-orbit interaction, Nat. Phys. **6**, 376 (2010).
[19] X.-L. Qi and S.-C. Zhang, Topological insulators and superconductors, Rev. Mod. Phys. **83**, 1057 (2011).
[20] M. Zahid Hasan and C. L. Kane, Colloquium: Topological insulators, Rev. Mod. Phys. **82**, 3045 (2010).
[21] D. A. Ivanov, Non-Abelian Statistics of Half-Quantum Vortices in p-Wave Superconductors, Phys. Rev. Lett. **86**, 268 (2001).
[22] A Yu Kitaev, Fault-tolerant quantum computation by anyons, Ann. Phys. (Amsterdam) **303**, 2 (2003).
[23] C. Nayak, S. H. Simon, A. Stern, M. Freedman, and S. Das Sarma, Non-Abelian anyons and topological quantum computation, Rev. Mod. Phys. **80**, 1083 (2008).
[24] J. Alicea, New directions in the pursuit of Majorana fermions in solid state systems, Rep. Prog. Phys. **75**, 076501 (2012).
[25] B. Lian, X.-Q. Sun, A. Vaezi, X.-L. Qi, and S.-C. Zhang, Topological quantum computation based on chiral Majorana fermions, Proc. Natl. Acad. Sci. U.S.A. **115**, 10938 (2018).
[26] M. Sato, Topological odd-parity superconductors, Phys. Rev. B **81**, 220504(R) (2010).
[27] L. Fu and E. Berg, Odd-Parity Topological Superconductors: Theory and Application to $Cu_xBi_2Se_3$, Phys. Rev. Lett. **105**, 097001 (2010).
[28] G. E. Volovik, Fermion zero modes on vortices in chiral superconductors, J. Exp. Theor. Phys. Lett. **70**, 609 (1999).
[29] N. Read and D. Green, Paired states of fermions in two dimensions with breaking of parity and time-reversal symmetries and the fractional quantum Hall effect, Phys. Rev. B **61**, 10267 (2000).
[30] A Yu Kitaev, Unpaired Majorana fermions in quantum wires, Phys. Usp. **44**, 131 (2001).
[31] S. Yonezawa, K. Tajiri, S. Nakata, Y. Nagai, Z. Wang, K. Segawa, Y. Ando, and Y. Maeno, Thermodynamic evidence for nematic superconductivity in $Cu_xBi_2Se_3$, Nat. Phys. **13**, 123 (2017).
[32] L. Fu and C. L. Kane, Superconducting Proximity Effect and Majorana Fermions at the Surface of a Topological Insulator, Phys. Rev. Lett. **100**, 096407 (2008).
[33] Y. Oreg, G. Refael, and F. von Oppen, Helical Liquids and Majorana Bound States in Quantum Wires, Phys. Rev. Lett. **105**, 177002 (2010).
[34] R. M. Lutchyn, J. D. Sau, and S. Das Sarma, Majorana Fermions and a Topological Phase Transition in Semiconductor-Superconductor Heterostructures, Phys. Rev. Lett. **105**, 077001 (2010).
[35] M. Sato, Y. Takahashi, and S. Fujimoto, Non-Abelian Topological Order in s-Wave Superfluids of Ultracold Fermionic Atoms, Phys. Rev. Lett. **103**, 020401 (2009).
[36] J. D. Sau, R. M. Lutchyn, S. Tewari, and S. Das Sarma, Generic New Platform for Topological Quantum Computation Using Semiconductor Heterostructures, Phys. Rev. Lett. **104**, 040502 (2010).
[37] J. Alicea, Majorana fermions in a tunable semiconductor device, Phys. Rev. B **81**, 125318 (2010).
[38] C. L. M. Wong and K. T. Law, Majorana Kramers doublets in $d_{x^2-y^2}$-wave superconductors with Rashba spin-orbit coupling, Phys. Rev. B **86**, 184516 (2012).
[39] F. Zhang, C. L. Kane, and E. J. Mele, Time-Reversal-Invariant Topological Superconductivity and Majorana Kramers Pairs, Phys. Rev. Lett. **111**, 056402 (2013).
[40] V. Mourik, K. Zuo, S. M. Frolov, S. R. Plissard, E. P. A. M. Bakkers, and L. P. Kouwenhoven, Signatures of Majorana fermions in hybrid superconductor-semiconductor nanowire devices, Science **336**, 1003 (2012).
[41] A. Das, Y. Ronen, Y. Most, Y. Oreg, M. Heiblum, and H. Shtrikman, Zero-bias peaks and splitting in an Al-InAs nanowire topological superconductor as a signature of Majorana fermions, Nat. Phys. **8**, 887 (2012).
[42] L. P. Rokhinson, X. Liu, and J. K. Furdyna, The fractional a.c. Josephson effect in a semiconductor-superconductor nanowire as a signature of Majorana particles, Nat. Phys. **8**, 795 (2012).
[43] M. T. Deng, C. L. Yu, G. Y. Huang, M. Larsson, P. Caroff, and H. Q. Xu, Anomalous zero-bias conductance peak in a Nb-InSb nanowire-Nb hybrid device, Nano Lett. **12**, 6414 (2012).
[44] S. Nadj-Perge, I. K. Drozdov, J. Li, H. Chen, S. Jeon, J. Seo, A. H. MacDonald, B. A. Bernevig, and A. Yazdani, Observation of Majorana fermions in ferromagnetic atomic chains on a superconductor, Science **346**, 602 (2014).
[45] H. Zhang *et al.*, Quantized Majorana conductance, Nature (London) **556**, 74 (2018).
[46] H.-H. Sun, K.-W. Zhang, L.-H. Hu, C. Li, G.-Y. Wang, H.-Y. Ma, Z.-A. Xu, C.-L. Gao, D.-D. Guan, Y.-Y. Li, C. Liu, D. Qian, Y. Zhou, L. Fu, S.-C. Li, F.-C. Zhang, and J.-F. Jia, Majorana Zero Mode Detected with Spin Selective Andreev Reflection in the Vortex of a Topological Superconductor, Phys. Rev. Lett. **116**, 257003 (2016).
[47] D. Wang, L. Kong, P. Fan, H. Chen, S. Zhu, W. Liu, L. Cao, Y. Sun, S. Du, J. Schneeloch *et al.*, Evidence for Majorana bound states in an iron-based superconductor, Science **362**, 333 (2018).
[48] R. M. Lutchyn, E. P. A. M. Bakkers, L. P. Kouwenhoven, P. Krogstrup, C. M. Marcus, and Y. Oreg, Majorana zero modes in superconductor-semiconductor heterostructures, Nat. Rev. Mater. **3**, 52 (2018).
[49] W. A. Benalcazar, B. Andrei Bernevig, and T. L. Hughes, Quantized electric multipole insulators, Science **357**, 61 (2017).
[50] W. A. Benalcazar, B. Andrei Bernevig, and T. L. Hughes, Electric multipole moments, topological multipole moment pumping, and chiral hinge states in crystalline insulators, Phys. Rev. B **96**, 245115 (2017).
[51] F. Schindler, A. M. Cook, M. G. Vergniory, Z. Wang, S. S. P. Parkin, B. Andrei Bernevig, and T. Neupert, Higher-order topological insulators, Sci. Adv. **4**, eaat0346 (2018).
[52] X. Zhu, Second-Order Topological Superconductors with Mixed Pairing, Phys. Rev. Lett. **122**, 236401 (2019).
[53] J. Langbehn, Y. Peng, L. Trifunovic, F. von Oppen, and P. W. Brouwer, Reflection-Symmetric Second-Order Topological Insulators and Superconductors, Phys. Rev. Lett. **119**, 246401 (2017).

[54] M. Ezawa, Higher-Order Topological Insulators and Semimetals on the Breathing Kagome and Pyrochlore Lattices, Phys. Rev. Lett. **120**, 026801 (2018).

[55] E. Khalaf, Higher-order topological insulators and superconductors protected by inversion symmetry, Phys. Rev. B **97**, 205136 (2018).

[56] M. Geier, L. Trifunovic, M. Hoskam, and P. W. Brouwer, Second-order topological insulators and superconductors with an order-two crystalline symmetry, Phys. Rev. B **97**, 205135 (2018).

[57] S. Franca, J. van den Brink, and I. C. Fulga, An anomalous higher-order topological insulator, Phys. Rev. B **98**, 201114(R) (2018).

[58] D. Călugăru, V. Juričić, and B. Roy, Higher-order topological phases: A general principle of construction, Phys. Rev. B **99**, 041301(R) (2019).

[59] F. Schindler, Z. Wang, M. G. Vergniory, A. M. Cook, A. Murani, S. Sengupta, A. Yu Kasumov, R. Deblock, S. Jeon, I. Drozdov *et al.*, Higher-order topology in bismuth, Nat. Phys. **14**, 918 (2018).

[60] S. Imhof, C. Berger, F. Bayer, J. Brehm, L. W. Molenkamp, T. Kiessling, F. Schindler, C. Hua Lee, M. Greiter, T. Neupert *et al.*, Topolectrical-circuit realization of topological corner modes, Nat. Phys. **14**, 925 (2018).

[61] M. Serra-Garcia, V. Peri, R. Süsstrunk, O. R. Bilal, T. Larsen, L. G. Villanueva, and S. D. Huber, Observation of a phononic quadrupole topological insulator, Nature (London) **555**, 342 (2018).

[62] C. W. Peterson, W. A. Benalcazar, T. L. Hughes, and G. Bahl, A quantized microwave quadrupole insulator with topologically protected corner states, Nature (London) **555**, 346 (2018).

[63] X. Zhang, H.-X. Wang, Z.-K. Lin, Y. Tian, B. Xie, M.-H. Lu, Y.-F. Chen, and J.-H. Jiang, Second-order topology and multidimensional topological transitions in sonic crystals, Nat. Phys. **15**, 582 (2019).

[64] J. Niu, T. Yan, Y. Zhou, Z. Tao, X. Li, W. Liu, L. Zhang, S. Liu, Z. Yan, Y. Chen *et al.*, Simulation of higher-order topological phases and related topological phase transitions in a superconducting qubit, arXiv:2001.03933.

[65] X. Zhu, Tunable Majorana corner states in a two-dimensional second-order topological superconductor induced by magnetic fields, Phys. Rev. B **97**, 205134 (2018).

[66] Z. Yan, F. Song, and Z. Wang, Majorana Kramers Pairs in a High-Temperature Platform, Phys. Rev. Lett. **121**, 096803 (2018).

[67] Y. Wang, M. Lin, and T. L. Hughes, Weak-pairing higher order topological superconductors, Phys. Rev. B **98**, 165144 (2018).

[68] Q. Wang, C.-C. Liu, Y.-M. Lu, and F. Zhang, High-Temperature Majorana Corner States, Phys. Rev. Lett. **121**, 186801 (2018).

[69] Z. Wu, Z. Yan, and W. Huang, Higher-order topological superconductivity: Possible realization in Fermi gases and Sr_2RuO_4, Phys. Rev. B **99**, 020508(R) (2019).

[70] C.-H. Hsu, P. Stano, J. Klinovaja, and D. Loss, Majorana Kramers Pairs in Higher-Order Topological Insulators, Phys. Rev. Lett. **121**, 196801 (2018).

[71] T. Liu, J. J. He, and F. Nori, Majorana corner states in a two-dimensional magnetic topological insulator on a high-temperature superconductor, Phys. Rev. B **98**, 245413 (2018).

[72] Y. Volpez, D. Loss, and J. Klinovaja, Second-Order Topological Superconductivity in π-Junction Rashba Layers, Phys. Rev. Lett. **122**, 126402 (2019).

[73] R.-X. Zhang, W. S. Cole, and S. Das Sarma, Helical Hinge Majorana Modes in Iron-Based Superconductors, Phys. Rev. Lett. **122**, 187001 (2019).

[74] Y. Peng and Y. Xu, Proximity-induced Majorana hinge modes in antiferromagnetic topological insulators, Phys. Rev. B **99**, 195431 (2019).

[75] C. Zeng, T. D. Stanescu, C. Zhang, V. W. Scarola, and S. Tewari, Majorana Corner Modes with Solitons in an Attractive Hubbard-Hofstadter Model of Cold Atom Optical Lattices, Phys. Rev. Lett. **123**, 060402 (2019).

[76] Z. Yan, Higher-Order Topological Odd-Parity Superconductors, Phys. Rev. Lett. **123**, 177001 (2019).

[77] Z. Yan, Majorana corner and hinge modes in second-order topological insulator/superconductor heterostructures, Phys. Rev. B **100**, 205406 (2019).

[78] S. Ali Akbar Ghorashi, X. Hu, T. L. Hughes, and E. Rossi, Second-order Dirac superconductors and magnetic field induced Majorana hinge modes, Phys. Rev. B **100**, 020509 (R) (2019).

[79] S.-B. Zhang and B. Trauzettel, Detection of second-order topological superconductors by Josephson junctions, Phys. Rev. Research **2**, 012018 (2020).

[80] X.-H. Pan, K.-J. Yang, L. Chen, G. Xu, C.-X. Liu, and X. Liu, Lattice-Symmetry-Assisted Second-Order Topological Superconductors and Majorana Patterns, Phys. Rev. Lett. **123**, 156801 (2019).

[81] K. Laubscher, D. Loss, and J. Klinovaja, Fractional topological superconductivity and parafermion corner states, Phys. Rev. Research **1**, 032017 (2019).

[82] S. Franca, D. V. Efremov, and I. C. Fulga, Phase-tunable second-order topological superconductor, Phys. Rev. B **100**, 075415 (2019).

[83] R.-X. Zhang, W. S. Cole, X. Wu, and S. Das Sarma, Higher-Order Topology and Nodal Topological Superconductivity in Fe(Se,Te) Heterostructures, Phys. Rev. Lett. **123**, 167001 (2019).

[84] J. Ahn and B.-J. Yang, Higher-order topological superconductivity of spin-polarized fermions, Phys. Rev. Research **2**, 012060 (2020).

[85] M. Kheirkhah, Y. Nagai, C. Chen, and F. Marsiglio, Majorana corner flat bands in two-dimensional second-order topological superconductors, Phys. Rev. B **101**, 104502 (2020).

[86] S. Ali Akbar Ghorashi, T. L. Hughes, and E. Rossi, Vortex and surface phase transitions in superconducting higher-order topological insulators, arXiv:1909.10536.

[87] Y.-J. Wu, J. Hou, X. Luo, Y. Li, and C. Zhang, In-Plane Zeeman Field Induced Majorana Corner and Hinge Modes in an s-Wave Superconductor Heterostructure, Phys. Rev. Lett. **124**, 227001 (2020).

[88] X. Wu, X. Liu, R. Thomale, and C.-X. Liu, High-T_c superconductor Fe(Se,Te) monolayer: An intrinsic, scalable and electrically-tunable Majorana platform, arXiv:1905.10648.

[89] Y.-T. Hsu, W. S. Cole, R.-X. Zhang, and J. D. Sau, Inversion-protected higher order topological superconductivity in monolayer WTe_2, arXiv:1904.06361.

[90] M. S. Scheurer and J. Schmalian, Topological superconductivity and unconventional pairing in oxide interfaces, Nat. Commun. **6**, 6005 (2015).

[91] A. Greco and A. P. Schnyder, Mechanism for Unconventional Superconductivity in the Hole-Doped Rashba-Hubbard Model, Phys. Rev. Lett. **120**, 177002 (2018).

[92] C. Zhang, S. Tewari, R. M. Lutchyn, and S. Das Sarma, $p_x + ip_y$ Superfluid from s-Wave Interactions of Fermionic Cold Atoms, Phys. Rev. Lett. **101**, 160401 (2008).

[93] M. Gong, G. Chen, S. Jia, and C. Zhang, Searching for Majorana Fermions in 2D Spin-Orbit Coupled Fermi Superfluids at Finite Temperature, Phys. Rev. Lett. **109**, 105302 (2012).

[94] S.-L. Zhu, L.-B. Shao, Z. D. Wang, and L.-M. Duan, Probing Non-Abelian Statistics of Majorana Fermions in Ultracold Atomic Superfluid, Phys. Rev. Lett. **106**, 100404 (2011).

[95] X.-J. Liu and H. Hu, Topological superfluid in one-dimensional spin-orbit-coupled atomic Fermi gases, Phys. Rev. A **85**, 033622 (2012).

[96] Z. Yan, S. Wan, and Z. Wang, Topological superfluid and Majorana zero modes in synthetic dimension, Sci. Rep. **5**, 15927 (2015).

[97] R. Micnas, J. Ranninger, and S. Robaszkiewicz, Superconductivity in narrow-band systems with local nonretarded attractive interactions, Rev. Mod. Phys. **62**, 113 (1990).

[98] H. Tsuchiura, Y. Tanaka, and Y. Ushijima, Stability of $s + id$-wave pairing state in the 2D extended Hubbard model, J. Phys. Soc. Jpn. **64**, 922 (1995).

[99] J. Hutchinson and F. Marsiglio, Superconducting order parameter symmetry for the extended Hubbard model below T_c, arXiv:1902.08316.

[100] See Supplemental Material at http://link.aps.org/supplemental/10.1103/PhysRevLett.125.017001 for details of the derivation of various results, which includes Refs. [37,76].

[101] Here, by pure s-wave pairing we mean $\Delta_0 + \Delta_s \eta_s(\boldsymbol{k})$ when at least one of the Δ_0 or Δ_s values is finite. It should be noted that pure s-wave pairing has pairing line nodes only when $|\Delta_0/\Delta_s| \leq 1$.

[102] X.-L. Qi, T. L. Hughes, and S.-C. Zhang, Topological invariants for the Fermi surface of a time-reversal-invariant superconductor, Phys. Rev. B **81**, 134508 (2010).

[103] Here, $\mathbb{Z}_2$ invariant is defined as $\nu = \prod_i [\mathrm{sgn}(\Delta_i)]^{m_i}$ where $\mathrm{sgn}(\Delta_i)$ represents the sign of the pairing on the ith spin-split FS, and m_i denotes the number of time-reversal invariant points within the ith FS.

[104] C.-K. Chiu, J. C. Y. Teo, A. P. Schnyder, and S. Ryu, Classification of topological quantum matter with symmetries, Rev. Mod. Phys. **88**, 035005 (2016).

[105] Another important point is that if the normal state of a superconductor does not have a FS, the underlying topology must be trivial since such a phase can continuously transform to the limit $|\mu| \to \infty$ without the closing of either the bulk or the boundary gap.

[106] When the Fermi surface is anisotropic, it is a general feature that topologically trivial and second-order topological $s + id$-wave phases are separated by an intervening first-order topological phase. This fact can be understood by inspecting the configurations of both Fermi surfaces and pairing nodes. It is not hard to see that, when the Fermi surface is anisotropic, the four pairing nodes can not simultaneously move outside all Fermi surfaces.

[107] J. Nitta, T. Akazaki, H. Takayanagi, and T. Enoki, Gate Control of Spin-Orbit Interaction in an Inverted $In_{0.53}Ga_{0.47}As/In_{0.52}Al_{0.48}As$ Heterostructure, Phys. Rev. Lett. **78**, 1335 (1997).

[108] W.-C. Lee, S.-C. Zhang, and C. Wu, Pairing State with a Time-Reversal Symmetry Breaking in FeAs-Based Superconductors, Phys. Rev. Lett. **102**, 217002 (2009).

[109] G. R. Stewart, Superconductivity in iron compounds, Rev. Mod. Phys. **83**, 1589 (2011).

[110] R. P. Day, G. Levy, M. Michiardi, B. Zwartsenberg, M. Zonno, F. Ji, E. Razzoli, F. Boschini, S. Chi, R. Liang, P. K. Das, I. Vobornik, J. Fujii, W. N. Hardy, D. A. Bonn, I. S. Elfimov, and A. Damascelli, Influence of Spin-Orbit Coupling in Iron-Based Superconductors, Phys. Rev. Lett. **121**, 076401 (2018).

[111] N. Reyren, S. Thiel, A. D. Caviglia, L. F. Kourkoutis, G. Hammerl, C. Richter, C. W. Schneider, T. Kopp, A.-S. Rüetschi, D. Jaccard *et al.*, Superconducting interfaces between insulating oxides, Science **317**, 1196 (2007).

[112] M. Ben Shalom, M. Sachs, D. Rakhmilevitch, A. Palevski, and Y. Dagan, Tuning Spin-Orbit Coupling and Superconductivity at the $SrTiO_3/LaAlO_3$ Interface: A Magnetotransport Study, Phys. Rev. Lett. **104**, 126802 (2010).

[113] J. D. Sau, R. Sensarma, S. Powell, I. B. Spielman, and S. Das Sarma, Chiral Rashba spin textures in ultracold Fermi gases, Phys. Rev. B **83**, 140510(R) (2011).